Proceedings of the CAS-CERN Accelerator School: Intensity Limitations in Particle Beams, Geneva, Switzerland, 2–11 November 2015, edited by W. Herr, CERN Yellow Reports: School Proceedings, Vol. 3/2017, CERN-2017-006-SP (CERN, Geneva, 2017)

Beam-Based Impedance Measurements

E. Shaposhnikova
CERN, Geneva, Switzerland

Abstract

Beam-based impedance measurements play an important role in benchmarking existing impedance models of the accelerator, as well as in elaborating them. Impedance measurements can be made with both stable and unstable beams. In the first case, one makes use of changes in stable bunch parameters, such as bunch length, synchrotron frequency distribution, or synchronous phase shift. In the second case, measurements of instability characteristics (threshold, growth rates, bunch spectrum) can be used for impedance search or evaluation, usually by comparison with results of particle simulations.

Keywords

Impedance; beam measurements.

1 Introduction

First of all, let us answer the question; why does one need to measure impedance with a beam? Indeed, nowadays the beam-coupling impedance of various machine elements can be accurately estimated using analytical calculations [1, 2], advanced electromagnetic simulations (various codes are available), or bench measurements in the lab, e.g., see Refs. [3, 4].

Nevertheless, very often one needs to verify the accuracy of an impedance model, based on electromagnetic simulations or measurements, since there are always some very complex machine elements with impedances that are difficult to calculate, simulate, or measure; the material properties of these elements are also not always well known. In addition, non-conformities may also exist, from either fabrication errors or beam-induced damage owing to e.g., operation with high-intensity beams. Measurements with the beam can also be useful in identifying impedance sources that are driving beam instabilities or posing some other intensity limitations.

In what follows, we consider methods mainly used in circular proton accelerators with relatively high beam energy (above the gigaelectronvolt range) and long bunches (above the nanosecond range). The frequency ranges of interest for impedance measurements, and therefore the approaches used in these machines, are quite different from those applied in the synchrotron light sources with picosecond or even femtosecond bunches. Thanks to careful initial design, the impedances of modern rings become smaller and smaller, so that more elaborate methods are required to measure them with beam. However, numerical simulations of various collective effects have also become more advanced and can be used for comparison with beam tests of impedance.

Note that practically all intensity effects could potentially be used for impedance evaluation by comparison of beam measurements with particle simulations or analytical formulae. Only a few methods could be discussed in detail in this paper. Their selection is based on personal experience in using them on CERN machines and also on the fact that some of them are probably less well known outside CERN. Most of the examples are given for measurements in the longitudinal plane, but similar techniques are often applicable in the transverse plane.

This paper consists of two main parts. The first describes measurements with stable bunches that include bunch lengthening, synchrotron frequency shift, and change in debunching time with intensity, and are applied for evaluation of the reactive impedance $\mathrm{Im}Z$. Measurements of synchronous phase shift with intensity can be used to estimate the resistive part of the beam-coupling impedance $\mathrm{Re}Z$. The

https://doi.org/10.23730/CYRSP-2017-003.107

second part of the paper deals with an unstable beam and its characteristics (spectra, growth rates, and thresholds). In all these cases, the impedance evaluation is based on changes in beam characteristics. However, measurements with stable beams are mainly used to test the existing impedance models while measurements with unstable beams often contain important information about parameters of the dominant offending impedance. There is also a separate case (not considered in this paper) when the impedance of a particular element in the ring (e.g., an RF cavity) can be evaluated from the signal excited there by a single bunch with known (measured) profile (see, e.g., Ref. [5,6]). This approach can be considered an intermediate case between beam measurements and bench measurements of impedance in the lab, since the beam characteristics stay unchanged.

Measurements of impedance with a single bunch can give information only about the effective impedance—the actual impedance integrated over the spectrum of the bunch. For a stable bunch, the effective impedance is defined by integration over the stable bunch spectrum centred at zero frequency. Since the width of the bunch spectrum is inversely proportional to the bunch length τ, long bunches 'see' only the low-frequency ($f < 1/\tau$) part of the coupling impedance. For an unstable bunch, the situation is different. The growth rate of some mode depends on the effective impedance, which is now defined by integration over the spectrum of this mode with a non-zero centre frequency.

The total voltage seen by a particle is the sum of the RF voltage $V_{\rm rf}$ and the induced voltage $V_{\rm ind}$,

$$V = V_{\rm rf} + V_{\rm ind}\,. \tag{1}$$

The induced voltage due to beam-coupling impedance $Z(\omega)$ contains two contributions: the first defined by the stable bunch spectrum $\Lambda(\omega)$ and the second by the unstable spectrum $h(\omega)$. In the next section, we will consider the intensity effects defined by the stable bunch spectrum; in Section 3, we will consider the those defined by the unstable spectrum.

2 Impedance measurements with stable beam

In equilibrium, the particle distribution is a function of the Hamiltonian H with a potential well defined by the total voltage (1) seen by the particle (the effect of potential well distortion). The induced voltage can be written in the following form (see, e.g., Refs [7, 8]):

$$V_{\rm ind}(\theta) = -e\omega_0 N_{\rm b} \sum_n \Lambda_n Z_n {\rm e}^{{\rm i}n\theta}\,, \tag{2}$$

where $\omega_0 = 2\pi f_0$ is the revolution frequency, θ is the longitudinal co-ordinate of the particle expressed in radians, $Z_n = Z(n\omega_0)$, and

$$\Lambda_n = \frac{1}{2\pi}\int \lambda(\theta){\rm e}^{-{\rm i}n\theta}{\rm d}\theta \tag{3}$$

is the nth Fourier harmonic of the unperturbed bunch line density $\lambda(\theta)$ containing $N_{\rm b}$ particles and normalized to unity

$$\int \lambda(\theta){\rm d}\theta = 1\,. \tag{4}$$

Equation (2) is sufficient to obtain, in a self-consistent way, the equilibrium particle distribution, which provides measurable dependence of synchrotron frequency $\omega_{\rm s}$, bunch length τ, and synchronous phase on bunch intensity. The Haissinski equation describes the situation for an electron bunch in equilibrium, assuming the Gaussian distribution in energy [9]. However, there is no unique solution for proton bunches and measured bunch profiles should be used to obtain the required equilibrium bunch characteristics.

Assuming a symmetric bunch profile with $\Lambda_n = \Lambda_{-n}$, Eq. (2) becomes

$$V_{\rm ind}(\theta) = -2\pi I_{\rm b} \sum_n \Lambda_n ({\rm Re}Z_n \cos n\theta - {\rm Im}Z_n \sin n\theta)\,, \tag{5}$$

where $I_\mathrm{b} = ef_0N_\mathrm{b}$ is the average beam current. For $n\theta \ll 1$, the right-hand side of Eq. (5) can be expanded to give

$$V_\mathrm{ind}(\theta) \simeq -2\pi I_\mathrm{b} \sum_n \Lambda_n(\mathrm{Re}Z_n - n\theta\,\mathrm{Im}Z_n + ...)\,, \tag{6}$$

with $\mathrm{Re}Z$ leading to the synchronous phase shift and $\mathrm{Im}Z$ contributing to the change of the RF voltage amplitude and, therefore, introducing the synchrotron frequency shift.

Adding the induced voltage to the RF voltage in the linearized longitudinal equation of motion yields

$$\frac{\mathrm{d}^2\theta}{\mathrm{d}t^2} + \omega_{\mathrm{s}0}^2\left[\theta + \frac{V_\mathrm{ind}(\theta)}{V_\mathrm{rf}\,h\cos\phi_\mathrm{s}}\right] = 0\,, \tag{7}$$

where ϕ_s is the synchronous phase ($\phi = h\theta$, with RF harmonic number h) and $\omega_{\mathrm{s}0}$ is the synchrotron frequency of particles with small oscillation amplitude.

In this approximation, we get the following expression for the synchronous phase shift:

$$\Delta\phi_\mathrm{s} = h\Delta\theta \simeq \frac{2\pi I_\mathrm{b}}{V_\mathrm{rf}\cos\phi_\mathrm{s}} \sum_n \Lambda_n\,\mathrm{Re}Z_n\,, \tag{8}$$

which will be discussed in the corresponding section.

For the linear synchrotron frequency, we obtain

$$\omega_\mathrm{s}^2 \simeq \omega_{\mathrm{s}0}^2\left(1 + \frac{2\pi I_\mathrm{b}}{V_\mathrm{rf}h\cos\phi_\mathrm{s}} \sum_n n\Lambda_n\,\mathrm{Im}Z_n\right)\,. \tag{9}$$

We notice already that a dominant space charge impedance ($\mathrm{Im}Z < 0$) below transition ($\cos\phi_\mathrm{s} > 0$) or inductive impedance above transition leads to negative frequency shift. Note that Eqs. (8)–(9) are applicable only for small-amplitude particles and the dependence of the measured synchrotron frequency shift and phase on beam parameters can, in reality, be much more complicated.

2.1 Frequency shifts

For a reactive impedance $\mathrm{Im}\mathrm{Z}_n/n$, which is constant over the stable bunch spectrum, and for small shifts $\Delta\omega_\mathrm{s} \ll \omega_{\mathrm{s}0}$, Eq. (9) can be rewritten in the form

$$\Delta\omega_\mathrm{s} = \omega_\mathrm{s} - \omega_{\mathrm{s}0} \simeq \frac{\pi I_\mathrm{b}\omega_{\mathrm{s}0}}{V_\mathrm{rf}h\cos\phi_\mathrm{s}}\mathrm{Im}Z/n \sum_n n^2\Lambda_n\,. \tag{10}$$

Using the fact that

$$\lambda(\theta) = \sum_n \Lambda_n \mathrm{e}^{-\mathrm{i}n\theta}\,, \tag{11}$$

one can see that, for small-amplitude particles, the sum in Eq. (10) can be replaced by the second derivative of the bunch line density $\lambda(\theta)$, and we obtain

$$\Delta\omega_\mathrm{s} \simeq -\frac{\pi I_\mathrm{b}\omega_{\mathrm{s}0}\mathrm{Im}Z/n}{V_\mathrm{rf}h\cos\phi_\mathrm{s}}\left.\frac{\mathrm{d}^2\lambda}{\mathrm{d}\theta^2}\right|_{\theta=0}\,, \tag{12}$$

where the second derivative is taken at the bunch centre.

Note that for a constant $\mathrm{Im}Z/n$, a similar formula can be obtained directly from the expression for induced voltage $V_\mathrm{ind} = -L\mathrm{d}I/\mathrm{d}t$, where $I(t)$ is the instantaneous beam current and the inductance L can be found from the expression $\mathrm{i}\omega_0 L = \mathrm{Im}Z/n$. Then, Eq. (2), rewritten for $\mathrm{Im}Z/n = \mathrm{const}$, can also be reproduced.

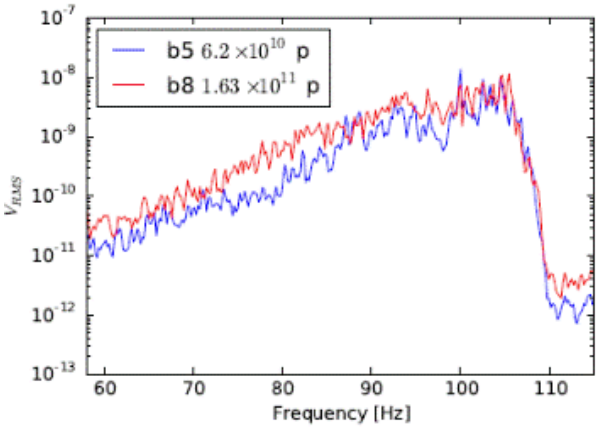

Fig. 1: Quadrupole line of peak-detected Schottky signal, proportional to particle distribution in synchrotron frequency, for two LHC bunches of Beam 1 with similar length of 1.4 ns (4σ Gaussian fit) but different intensities (0.1×10^{11} and 1.1×10^{11}) at 450 GeV/c ($f_{\mathrm{s0}} = 55.1$ Hz). The difference $2\delta f_{\mathrm{s}}$ is less than 1.0 Hz and $\delta f_{\mathrm{s}} = 0.35$ Hz is expected from the LHC impedance model [13].

For a parabolic bunch in a linear RF voltage, the expression for synchrotron frequency shift becomes particularly simple:

$$\omega_{\mathrm{s}}^2 = \omega_{\mathrm{s0}}^2 + \frac{6\omega_{\mathrm{s0}}^2 I_{\mathrm{b}} \mathrm{Im}Z/n}{V_{\mathrm{rf}} h \cos\phi_{\mathrm{s}} (\omega_0 \tau)^3} \,. \tag{13}$$

To obtain an estimate of $\mathrm{Im}Z/n$ of the ring, the synchrotron frequency shift should be measured as a function of bunch intensity N_{b}. Different possible methods are described next.

2.1.1 Incoherent synchrotron frequency shift

The incoherent synchrotron frequency shift can be found for a bunch in equilibrium by measuring the distance $2m\Delta f_{\mathrm{s}}$ between positive and negative mth synchrotron sidebands of the longitudinal Schottky spectrum [10]. This method was used in both RHIC rings [11], where the dependence on intensity was obtained from the natural intensity decay during luminosity production. The parabolas were fitted to the top 30% of the averaged bunch profiles to find $\mathrm{d}^2\lambda/\mathrm{d}\theta^2$. The results obtained by this method for the two RHIC rings, blue and yellow, which are very similar, differed by more than a factor of three; the source of this difference is not clear.

The quadrupole ($m = 2$) line of the peak-detected Schottky spectrum contains information about the particle distribution in synchrotron frequency [12] and can be used to observe the synchrotron frequency shift. The measurements of the $m = 2$ line performed at the bottom energy of the CERN LHC for two bunches of similar bunch length and different intensities are shown in Fig. 1. As one can see, the available frequency resolution of 0.2 Hz is insufficient and only an upper limit on $\mathrm{Im}Z/n$ could be obtained ($< 0.2\ \Omega$) [13]. This limit agrees with the current LHC impedance budget of $0.1\ \Omega$.

Another method that can be used to estimate the synchrotron frequency shift, when applied in the LHC, gave similar results. Eight bunches with intensities in the range 0.6×10^{11}–2.0×10^{11} and bunch length in the range 1.2–1.4 ns were excited via a cavity set point by phase modulation $\phi(t) = \phi_0 \sin(2\pi f_{\mathrm{mod}} t)$ with modulation frequency f_{mod}, changing in steps of 0.1 Hz from the zero-intensity synchrotron frequency $f_{\mathrm{s0}} = 55.1$ Hz. Dipole oscillations of different bunches were observed at excitation frequencies, reaching the synchrotron frequency spread inside these bunches. The results are again in agreement with an expected maximum frequency shift of 0.11 Hz. Owing to the finite length of this excitation (and therefore the frequency bandwidth), a constant offset in synchrotron frequencies was also observed. To improve accuracy, longer excitations were applied for shorter bunches (available at the LHC flat top) in recent machine studies. Finally, the LHC impedance ($\mathrm{Im}Z/n = 0.09\ \Omega$) could be

estimated most accurately from the measurements (using bunches with various lengths and intensities) of thresholds of the loss of Landau damping caused by the incoherent synchrotron frequency shift [13], but these results are not discussed here.

2.1.2 Coherent synchrotron frequency shift

The synchrotron frequency shift can also be measured from excited oscillations of bunches with different intensities N_b. In this case, we are dealing with the coherent synchrotron frequency shift as well as the incoherent shift, since now the bunch spectrum consists of both stationary and oscillating components. The frequency of bunch oscillations $\omega_m = 2\pi f_m$ can be presented in the form (see, e.g., Ref. [8])

$$\omega_m = m(\omega_{\mathrm{s}0} + \Delta\omega_\mathrm{inc}) + \Delta\omega_\mathrm{coh}\,, \tag{14}$$

where $\Delta\omega_\mathrm{inc}$ and $\Delta\omega_\mathrm{coh}$ are the incoherent and coherent synchrotron frequency shifts, respectively. The two last terms in Eq. (14) are defined by the two different effective impedances. Indeed, the incoherent frequency shift $\Delta\omega_\mathrm{inc} \propto \mathrm{Im}Z_0$ and the coherent frequency shift $\Delta\omega_\mathrm{inc} \propto (\mathrm{Im}Z/\omega)_m^\mathrm{eff}$, where

$$(\mathrm{Im}Z/\omega)_m^\mathrm{eff} = \frac{\sum_{p=-\infty}^{\infty} h_m(\omega_{pm}) Z(\omega_{pm})/\omega_{pm}}{\sum_{p=-\infty}^{\infty} h_m(\omega_{pm})} \tag{15}$$

and $\omega_{pm} = p\omega_0 + m\omega_s$.

For a Gaussian bunch with r.m.s. bunch length σ, the spectrum function is

$$h_m(\omega) = (\omega\sigma)^{2m} \mathrm{e}^{-(\omega\sigma)^2} \tag{16}$$

and

$$Z_0 \simeq \sum_{p=-\infty}^{\infty} p\,\mathrm{Im}Z(\omega_{p0}) \mathrm{e}^{-(\omega_{p0}\sigma)^2/2}\,. \tag{17}$$

For dipole oscillations ($m = 1$), the last two terms in Eq. (14) practically cancel each other (exactly, for a parabolic bunch in a linear RF voltage). Thus, for beam measurements we are left with quadrupole ($m = 2$) oscillations, which, for example, can be excited at injection into a mismatched RF voltage or by a non-adiabatic increase of voltage. The frequency of bunch length (or bunch peak amplitude) oscillations can be found from fitting the first 12–13 oscillations with a sine wave or from the maximum frequency in the peak-detected Schottky spectrum [14]. The variation of bunch intensity allows the dependence of oscillation frequency on impedance to be estimated using the expression

$$f_\mathrm{2s} = f_\mathrm{2s}(N_\mathrm{b} = 0) + bN_\mathrm{b}\,, \tag{18}$$

where for $\mathrm{Im}Z/n = \mathrm{const}$ the slope $b \propto \mathrm{Im}Z/n$ [7]. Note that the slope b also strongly depends on bunch length (as $1/\tau^3$ for $\mathrm{Im}Z/n = \mathrm{const}$) and special care should been taken when making the reference impedance measurements, as in the CERN SPS [14], by using bunches with similar bunch lengths and also emittances.

Indeed, single bunches injected into mismatched voltage at 26 GeV/c (above transition) have been used in the CERN SPS to evaluate changes in longitudinal inductive impedance since 1999, see Fig. 2 (left-hand side). The first significant reduction in the inductive impedance (the slope b) could be seen after shielding the $\sim$900 pumping ports in 2000 (compare measurements from 1999 and 2001). This was followed by an impedance increase due to installation in 2003 and 2006 of kickers for beam extraction to the two LHC rings. Later, the impedance of a few kickers was significantly reduced, but the effect was no longer measurable with the beam [14], mainly owing to variation of the injected bunch length (emittance) in measurements. Recently, measurements of synchrotron frequency shift as a function of bunch length allow the frequency dependence of effective impedances to be studied, see Fig. 2 (right-hand side). A comparison of these measurements with particle simulations can serve as a good test of

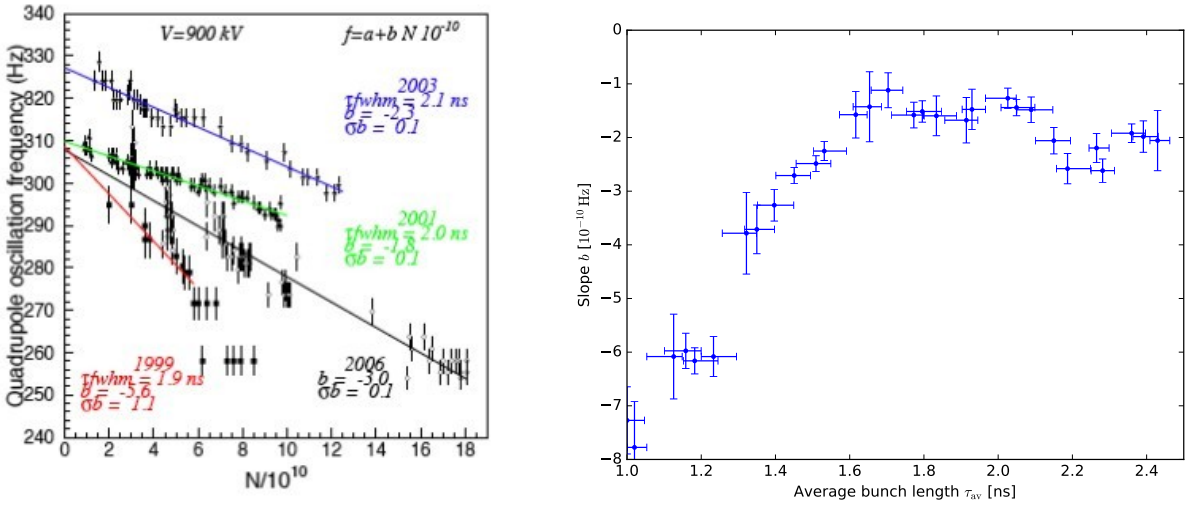

Fig. 2: Left-hand side: measurements of quadrupole frequency shift as a function of intensity (slope b) over a period of years in the CERN SPS following up the impedance evolution of the ring [14]. Right-hand side: recent measurements of the slope b from Eq. (18) in [Hz/10^{10}] as a function of average bunch length [15].

the impedance model of the ring. In the case of the CERN SPS, this comparison reveals some missing inductive impedance $\mathrm{Im}Z/n \sim 0.3\,\Omega$ [15]. The analysis also shows that for the SPS impedance measured using the quadrupole oscillations, the frequency shift in Eq. (14) is dominated by the contribution from the incoherent frequency shift.

Changes in the transverse SPS impedance were also observed over many years by performing measurements of the vertical tune shift with intensity [16].

2.2 Debunching

The voltage induced by the bunch produces 'potential well distortion' and changes the synchrotron frequency distribution when RF is on, but it also affects the beam dynamics when RF is off. The effective reactive impedance of the ring can then also be estimated by measuring the evolution of the bunch parameters during the debunching process [17].

For a parabolic bunch, the variation with time of length τ and the peak line density λ_p in the presence of reactive impedance $\mathrm{Im}Z = \mathrm{const}$ with RF off,

$$\tau(t) = \tau(0)\, r(t)\,, \qquad \lambda_\mathrm{p}(t) = \lambda_\mathrm{p}(0)/r(t)\,, \tag{19}$$

is described by the function $r(t)$. At the beginning of debunching, it has the form [18]

$$r(t) \simeq (1 + \Omega_\mathrm{d}^2 t^2)^{1/2}\,, \qquad \text{with} \quad \Omega_\mathrm{d}^2 = \Omega^2 + s\Omega_N^2\,, \tag{20}$$

where

$$\Omega = \frac{2|\eta|}{\tau(0)|}\frac{\Delta p_m}{p}\,, \qquad \Omega_N^2 = \frac{6N_\mathrm{b}e^2|\eta|}{\pi E\tau^3}\,\mathrm{Im}Z/n\,, \tag{21}$$

$\pm\Delta p_m/p$ is the maximum relative momentum spread in the bunch and $s = \mathrm{sign}(\eta \mathrm{Im}Z)$. The plus sign gives faster debunching, owing to the defocusing effect of inductive impedance above transition, or capacitive below transition, see Fig. 3 (top).

Here, the parameter Ω_N is similar to that contributing to the incoherent synchrotron frequency shift in Eq. (14). For $N_\mathrm{b} = 0$, the matched bunch has $\Omega = \omega_{\mathrm{s}0}$, otherwise it is defined by the RF parameters

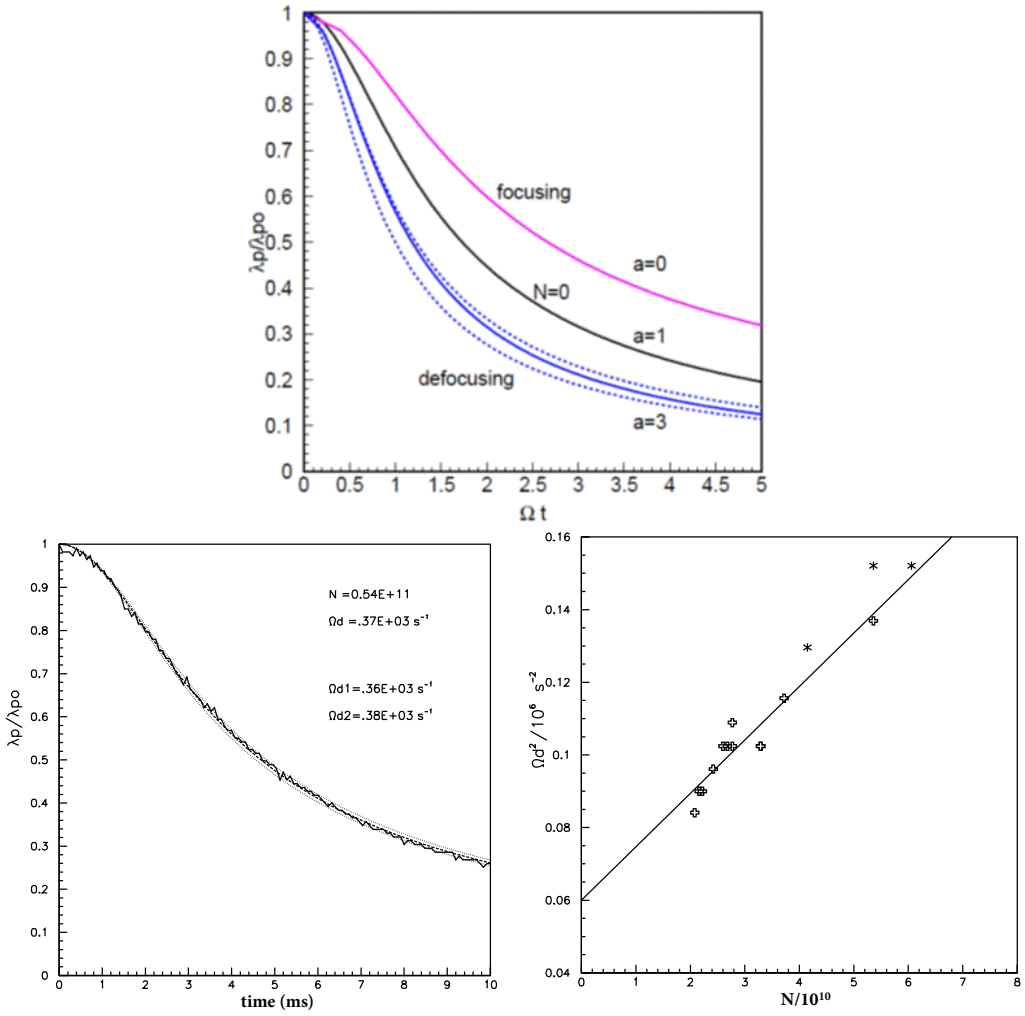

Fig. 3: Top: decay of normalized peak line density $1/r(t)$ with time for different values of parameter $a = 1 + 2s\,\Omega_N^2/\Omega^2$. $a = 1$ corresponds to absence of intensity effects. No debunching will happen for $a < 0$. Dashed lines are approximations of the exact solution valid at $t \ll 1/\Omega_\mathrm{d}$ and $t \gg 1/\Omega_\mathrm{d}$ [17]. Bottom left-hand side: example of measured peak line density variation during debunching in the SPS at 26 GeV/c and its fit using $r(t)$ from Eq. (20). Bottom right-hand side: measured Ω_d^2 as a function of intensity.

(synchrotron frequency) of the injector. This means that if the RF is switched off for a matched bunch with $\Omega^2 = \omega_{\mathrm{s}0}^2 - s\Omega_N^2$ then, as follows from Eq. (20), the debunching time $t_\mathrm{d} = 1/\Omega_\mathrm{d}$ in the first approximation does not depend on intensity.

The debunching time measured as a function of intensity from the decay of peak line density at 26 GeV/c in the CERN SPS is shown in Fig. 3. The estimate of $\mathrm{Im}Z/n$ (18.7 Ω) obtained by this method [17] is slightly larger than values found at that time (before the first impedance reduction) by other methods (with RF on), mainly because longer bunches during debunching sample lower frequencies and therefore a higher inductive impedance.

2.3 Bunch lengthening

Measurements of bunch lengthening with intensity under stable conditions are often used to estimate the effective reactive impedance of the ring. The Haissinski equation [9] describes the equilibrium bunch profile when, owing to the effect of synchrotron radiation, the momentum distribution is Gaussian, and therefore is normally applicable only in lepton machines.

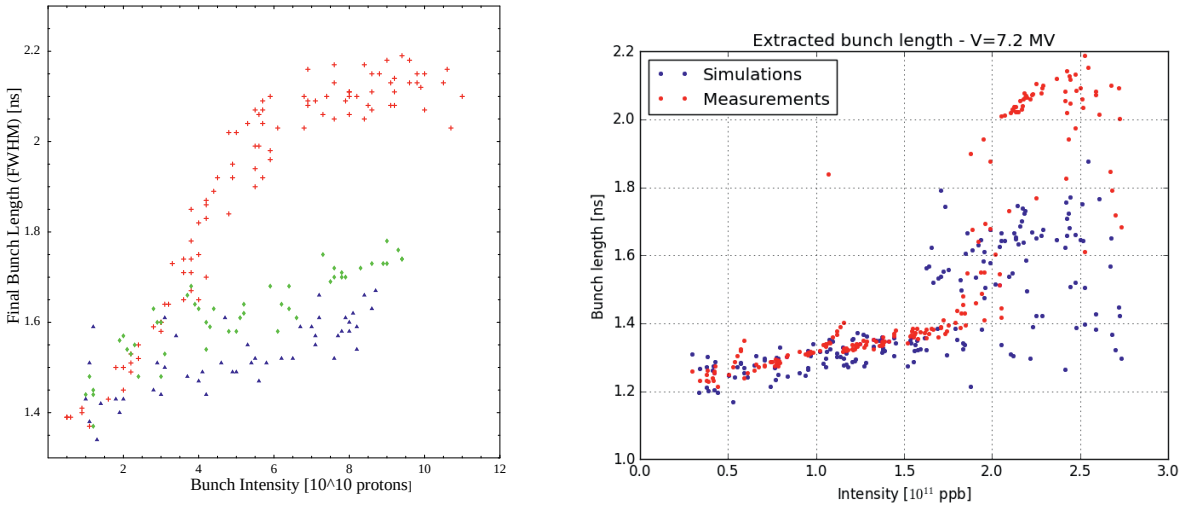

Fig. 4: Left-hand side: bunch length as a function of intensity on the 26 GeV/c SPS flat bottom at 600 ms after injection, before (red dots) and after (green and blue) the first impedance reduction in 1999–2001. Right-hand side: bunch length obtained from recent (2015) measurements (red) on the 450 GeV/c SPS flat top and macroparticle simulations through the whole acceleration cycle using initial bunch parameters from the measurements (blue) and full SPS impedance model [15].

The equation that describes bunch lengthening for protons [7] is based on the fact that longitudinal emittance is an invariant of motion. For parabolic bunches and constant inductive impedance $\mathrm{Im}Z/n$, the bunch length τ normalized to zero-intensity value τ_0 satisfies the following equation

$$\left(\frac{\tau}{\tau_0}\right)^4 + A\frac{\tau}{\tau_0} - 1 = 0\,, \qquad \text{where} \quad A = \frac{24\pi I_\mathrm{b}\mathrm{Im}Z/n}{(\omega_0\tau_0)^3 V_\mathrm{rf} h\cos\phi_\mathrm{s}}\,. \tag{22}$$

Comparison of measured and calculated bunch lengthening with intensity gives an estimate of reactive impedance, assuming $\mathrm{Im}Z/n = \mathrm{const}$. For proton bunches, the experiment is not easy, owing to the need for bunches with variable intensity but constant longitudinal emittance. If these bunches are injected into the ring, the constant RF voltage at injection can only be matched for a certain bunch intensity, leading at other intensities to quadrupole oscillations, filamentation, and emittance blow-up. Macroparticle simulations could be performed for the actual experimental set-up using longitudinal impedance having a more complicated, but realistic structure. Usually, bunch lengthening due to potential well distortion can be easily distinguished from that due to an instability; see two examples of SPS bunch lengthening measurements on the flat bottom and flat top in Fig. 4.

2.4 Synchronous phase shift

Measurements of the synchronous phase shift as a function of intensity are often used to evaluate the resistive impedance of the ring that abstracts particle energy [19]. In the absence of acceleration, the synchronous phase ϕ_s is defined by the expression

$$\Delta\phi_\mathrm{s} = -U/(e\,V_\mathrm{rf}\cos\phi_\mathrm{s})\,, \tag{23}$$

where U is the energy loss per turn and per particle.

Equation (8) describes the phase shift of a single particle with a small synchrotron oscillation amplitude. In the same way as energy loss of a given particle, this phase shift depends on particle oscillation amplitude. Experimentally, only the total energy loss of the whole bunch can be measured. The total energy loss normalized to the number of particles can be found by measuring the synchronous phase

shift $\Delta\phi_{\rm s}$ at different bunch intensities. The measured dependence of energy loss on bunch length can be compared with that calculated from the known resistive impedances and the given bunch distribution [20].

The energy loss of the whole bunch per turn and per particle can be found from the following expression [7]:

$$U = -e^2 N_{\rm b} k\,, \tag{24}$$

with the loss factor:

$$k = \frac{\omega_0}{\pi} \sum_{p=0}^{\infty} {\rm Re} Z(p\omega_0) |\Lambda(p\omega_0)|^2\,. \tag{25}$$

Finally, one obtains

$$\Delta\phi_{\rm s} = \frac{2 I_{\rm b}}{V_{\rm rf} \cos\phi_{\rm s}} \sum_{p=0}^{\infty} {\rm Re} Z(p\omega_0) |\Lambda(p\omega_0)|^2\,. \tag{26}$$

For a Gaussian bunch, the spectrum $\Lambda(\omega) = \exp[-(p\omega_0\sigma)^2/2]$ and one can see that Eq. (8) and Eq. (26) give the same result for $\sigma \ll 1/\omega_{\rm r}$.

The shift of the synchronous phase $\Delta\phi_{\rm s}$ can be measured from the distance between the two bunches in the ring or from the phase of the beam signal relative either to the reference RF signal or to the signal from a probe in the RF cavity. When using the reference RF signal (sent from the power amplifier to the cavity), the energy loss due to the cavity fundamental impedance is included. The signal from the probe in the cavity contains information about the sum of the applied RF voltage and the beam-induced voltage, so that in this case the beam-loading effect will be excluded from the measured phase shift. Measuring the distance between a time reference, low-intensity bunch and a witness bunch with varied intensity (see, e.g., Ref. [21]) is similar to the use of the reference RF signal, since the measured loss factor can be dominated by the contribution from the RF cavities.

Measurements of synchronous phase shift made in the CERN SPS after the first impedance reduction using the RF reference signal [22] are shown in Fig. 5. Single bunches with variable intensity were injected in four different RF voltages to obtain the dependence of energy loss on bunch length. In the measurements σ varied in the range 0.6–0.9 ns, so that impedances up to 1 GHz should be taken into account. Contributions to the normalized energy loss $\bar{U} = |U|/(N/10^{10})$ from different SPS impedances with frequencies less than 1 GHz (at the time of measurements) calculated for a Gaussian bunch are shown in Fig. 5 (left-hand side). As can be seen, in these measurements, the energy loss was dominated by the loss in the fundamental impedance of the 200 MHz RF system (shunt impedance $R_{\rm sh} \simeq 4.5\ \Omega$, quality factor $Q = 140$) and the MKE kickers. Contributions due to the main impedance of the 800 MHz cavities, total $R_{\rm sh} = 1.94$ MΩ and $Q = 300$, as well as the high-order mode of the 200 MHz RF system, with $f_{\rm r} = 629$ MHz, $Q = 500$ and $R_{\rm sh} = 604$ kΩ, are much smaller. The contribution to $\bar{U}$ from the resistive wall impedance is about 0.8 keV for a bunch with $\sigma = 0.6$ ns and decreases $\propto \sigma^{-3/2}$ for longer bunches. The measured and estimated total energy losses $\bar{U}$ are presented in Fig. 5 (right-hand side) as a function of bunch length.

The bunch-by-bunch measurements of the beam phase relative to the measured RF phase (probe) were used in the CERN LHC to estimate the energy loss of the proton bunches due to the electron cloud. Very high precision, within one degree, is required to measure the small shifts accurately. To obtain reliable results, the first 12 bunches were used as a reference to exclude other energy losses, from (short-range) impedances. The required accuracy was achieved after corrections for systematic errors and data post-processing [13]. Comparison with simulations gives a good estimate of the electron-cloud density [23]. This diagnostic tool has been available in the CERN Control Centre since 2015 and is used to evaluate results of beam scrubbing of the vacuum chamber, Fig. 6.

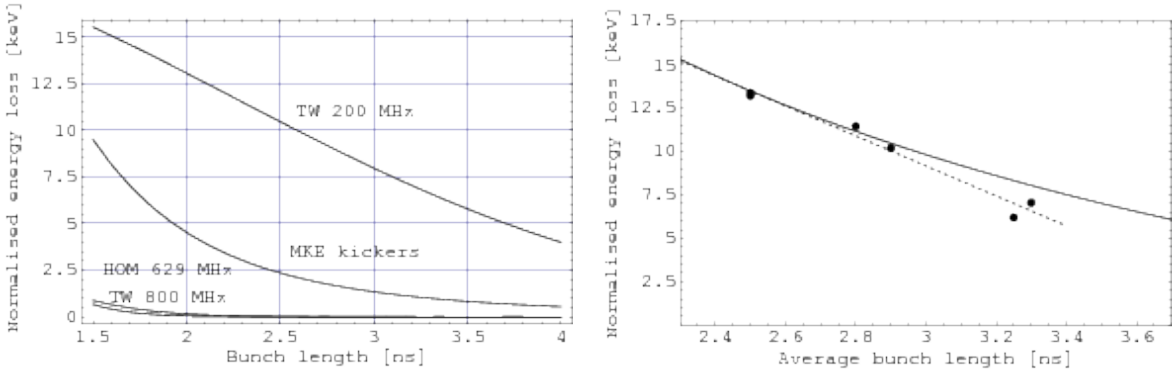

Fig. 5: Left-hand side: contribution to energy loss $\bar{U}$ (keV) from different SPS impedances as a function of 4σ bunch length. Right-hand side: normalized energy loss $\bar{U}$ (keV) calculated from the known SPS impedances (solid line) and measured from the phase shift (circles, measurement points; dashed line, linear fit) for different bunch lengths.

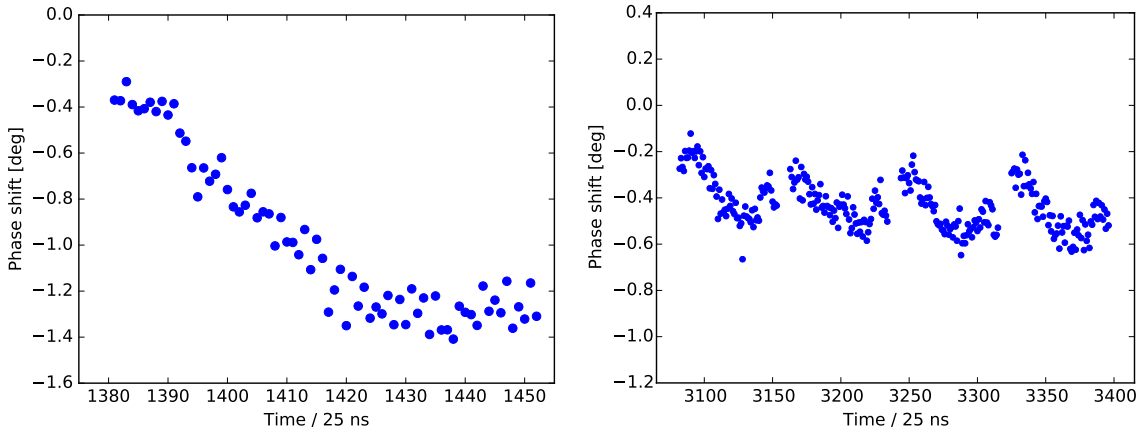

Fig. 6: Bunch-by-bunch synchronous phase shift for similar bunches spaced at 25 ns before (left-hand side) and after (right-hand side) scrubbing of the CERN LHC. Measurements at 450 GeV/c flat bottom [13].

3 Impedance measurements with unstable beam

Measurements with an unstable beam can help to identify the impedance source responsible for the instability. In particular, in some cases, which are considered next, the beam spectrum may contain important information about the frequency of the impedance responsible. Measurements of growth rates and instability thresholds are useful to estimate other parameters (R_{sh} and Q) of these impedances, especially with known resonant frequencies.

3.1 Unstable beam spectra with RF off: single-bunch case

Unstable spectra of long single bunches injected into an accelerator with RF off can be used to identify the longitudinal resonant impedances with large values of R/Q (for details see Refs. [24, 25]). The presence of different resonant impedances leads to line density modulation at the resonant frequencies, which can be detected. The synchrotron motion normally destroys this modulation (with the exception of a very fast instability with growth time significantly smaller then the synchrotron period). Too fast debunching will also modify this modulation. Thus, the parameters of bunches used for these measurements should satisfy certain requirements. For narrow-band resonant impedances with frequency bandwidth $\Delta\omega_{\mathrm{r}} \ll 1/\tau$, the width of the corresponding peak in the unstable spectrum is defined by $1/\tau$, so long bunches give better frequency resolution. Since injected bunches should become unstable, but not debunch too quickly, a

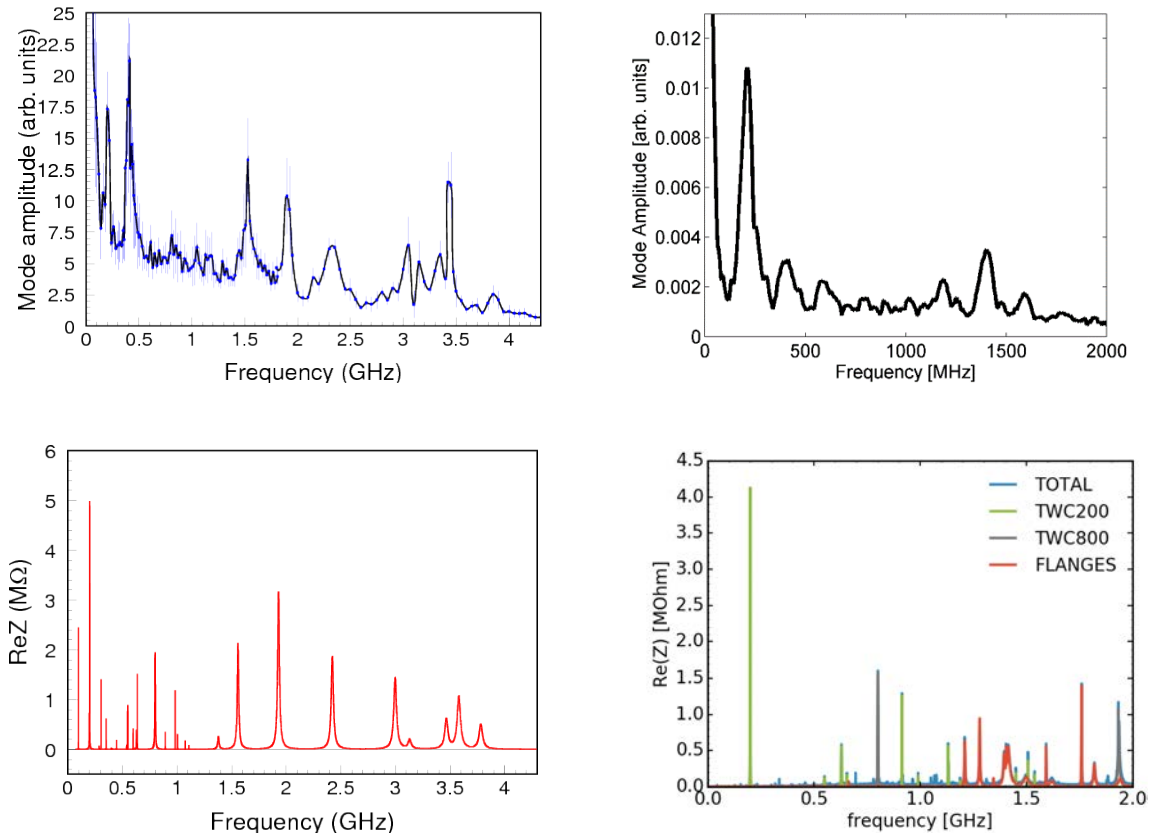

Fig. 7: Top: spectral distributions of long (25 ns) unstable bunches on the SPS flat bottom with RF off measured before the first SPS impedance reduction with $N_\mathrm{b} = 2 \times 10^{10}$ (left-hand side) and recently with $N_\mathrm{b} = 1 \times 10^{11}$. Bottom: corresponding longitudinal impedance models of the SPS; left-hand side: all resonant peaks above 1.4 GHz are due to intermagnet pumping ports shielded in 1999–2000 shutdown; right-hand side: impedance of vacuum flanges (blue) which will be reduced in the 2019–2020 shutdown.

small momentum spread also helps.

This method helped to find the impedances driving the microwave instability on the 26 GeV/c flat bottom in the CERN SPS almost 20 years ago, see Fig. 4 (left-hand side). Around 900 of the intermagnet pumping ports were shielded during the shutdown of 1999–2000, providing stability of the nominal LHC beam. Recently, this method (but with higher-intensity bunches) was used again in preparation of the SPS for its role as an injector of the high-luminosity LHC, where intensities that are twice as high as those achieved so far are required. The second impedance reduction programme, which includes shielding of $\sim$200 vacuum flanges, found responsible for a longitudinal instability during the SPS ramp (with minimum threshold on the flat top) [26, 27], is planned during the long shutdown in 2019–2020.

In the SPS measurements, bunch profiles were acquired during the first 100 ms after injection at regular time intervals. Each of these profiles was Fourier analysed and the maximum amplitude of the signal at each frequency was plotted (projection of mountain range). The spectral distributions measured with long bunches are shown in Fig. 7 (top), together with a corresponding impedance model at the time of measurement (bottom). Note the peak at 400 MHz, which disappeared after the first impedance reduction (shielding of pumping ports with resonant peaks in the range 1.5–3.5 GHz) and removal of the lepton equipment (SPS as LEP injector), although the particular impedance source was not identified.

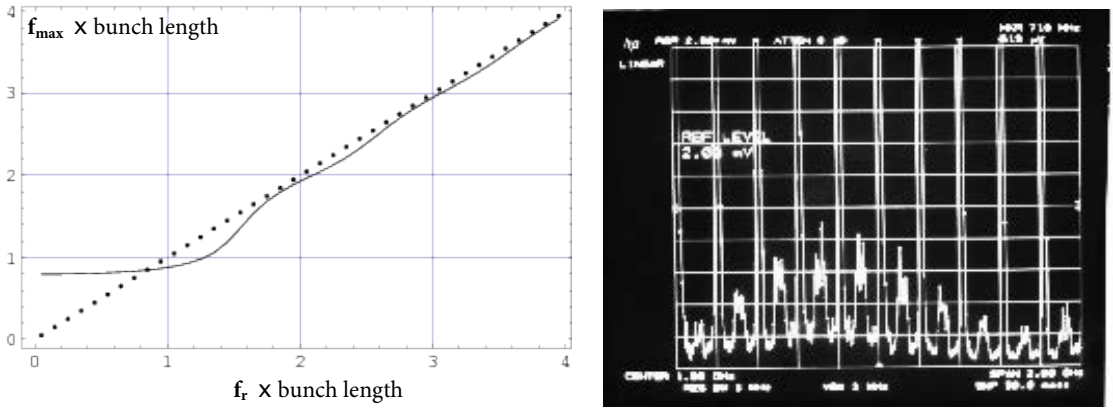

Fig. 8: Left-hand side: position of the maximum $f_{\max}\tau$ in the beam spectrum envelope as a function of $f_{\rm r}\tau$ for a parabolic line density and dipole mode $m = 1$. For higher multipoles m, the dependence is similar. Right-hand side: unstable beam spectrum from 0 to 2 GHz at the end of the fixed-target proton cycle in the CERN SPS for low-intensity beam (4×10^{12}) with 5 ns bunch spacing (strong lines at the 200 MHz harmonics).

3.2 Unstable beam spectra with RF on: multibunch case

Let us consider a coupled-bunch instability driven by some narrow-band impedance (e.g., high-order mode in the RF cavities) at resonant frequency $\omega_{\rm r} = 2\pi f_{\rm r} = \omega_0 p_{\rm r}$. The spectrum of the unstable multibunch beam has components at frequencies

$$\omega = (n + lM)\omega_0 + m\omega_{\rm s}, \quad l = 0, \pm 1, ..., \tag{27}$$

where M is the number of the equidistant bunches in the ring, $n = 0, 1, ..., M - 1$ is the coupled-bunch mode number describing the phase shift $2\pi n/M$ between adjacent bunches, and $m = 0, 1...$ is the multipole number related to the interbunch motion ($m = 1$, dipole; 2, quadrupole, and so on). On the spectrum analyser, the negative frequencies for a given value of n appear at $[(l + 1)M - n]\omega_0 - m\omega_{\rm s}$, so the spectrum is mirrored at $lM + n$ and $(l + 1)M - n$. With high-frequency resolution, one can use the fact that, above transition, internal synchrotron sidebands around revolution lines n and $M - n$ correspond to impedances at a higher frequency and external sidebands correspond to impedances at a lower frequency (the opposite is true below transition) [28]; however, the value of lM is still unknown. Measuring n for different (and, in particular, large) numbers of bunches M (with $M_1 \neq kM_2$) can also help to determine the resonant frequency $\omega_{\rm r}$. During development of the instability, the signals can also be directly observed from the coupling devices in the cavities.

Nevertheless, available data are often insufficient; then measurements of the envelope spectra can give additional information about the resonant frequency. The analysis of unstable beam spectra for different particle distribution functions has shown that if the measured position of the absolute maximum in the unstable bunch spectra $f_{\max} > 1/\tau$, then it practically coincides with the resonant frequency $f_{\rm r}$ [29]. The uncertainty does not exceed $\pm 0.2/\tau$. If the measured $f_{\max} < 1/\tau$, one can only say that $f_{\rm r} < 1.2/\tau$. The expected position of the maximum in the beam spectrum envelope as a function of resonant frequency is shown in Fig. 8 for a parabolic line density and $m = 1$ together with the spectrum envelope observed during development of a coupled-bunch instability in the CERN SPS for 4000 bunches spaced at 5 ns. From the measured value of $nf_0 = 113$ MHz, a few candidates were possible. Measurements were made at the end of the cycle for a bunch length of 2 ns. The spectrum has a maximum around 700 MHz so that the parameter $f_{\max}\tau = 1.4$. Then the driving impedance can be a high-order mode in the 200 MHz RF system with $f_{\rm r} = 912$ MHz.

Measurements of the instability growth rates and instability thresholds can be used to give an estimation of $R_{\rm sh}$ of the narrow-band impedance.

4 Discussion and summary

There are many other methods, for both transverse and longitudinal planes, which were not discussed here, see, for example, Refs. [20, 30].

Thanks to careful initial design, the coupling impedance of circular accelerators becomes smaller and therefore more elaborate methods are required to measure it with beams, even in proton machines (e.g., the LHC has $\mathrm{Im}Z/n = 0.09\ \Omega$). Numerical simulations of various collective effects also become more advanced and most of them can be also used for beam tests of impedance.

Measurements with stable beams are mainly used to verify existing impedance models. Conversely, measurements with unstable beams can provide important information about parameters of the dominant impedances driving the instabilities.

Acknowledgements

I am very grateful to all colleagues participating in beam impedance measurements in the CERN SPS and LHC, and in particular to T. Argyropoulos, T. Bohl, H. Damerau, A. Lasheen, T. Linnecar, J. Esteban Muller, and H. Timko.

References

[1] B.W. Zotter and S.A. Kheifets, *Impedances and Wakes in High-Energy Particle Accelerators* (World Scientific, Singapore, 1998). https://doi.org/10.1142/3068

[2] A. Chao, *Physics of Collective Beam Instabilities in High Energy Accelerators* (J. Wiley & Sons, New York, 1993).

[3] U. Niedermayer, Bench measurements and simulations of beam coupling impedance, these proceedings.

[4] R. Wanzerberg, Wakefields and impedances, these proceedings.

[5] J.M. Byrd *et al.*, *Nucl. Instrum. Methods Phys. Res. A* **455** (2000) 271. https://doi.org/10.1016/S0168-9002(00)00504-0

[6] J.M. Byrd, in *Handbook of Accelerator Physics and Engineering*, 2nd ed., Eds. A. Chao *et al.* (World Scientific, Singapore, 2013), p.750.

[7] B. Zotter, Potential-well bunch lengthening, CERN Report SPS-81-14-(DI) (1981).

[8] J.L. Laclare, Bunched beam coherent instabilities, Proc. CERN Accelerator School (CAS) 1985, CERN 87-03 (1987) p. 264.

[9] J. Haissinski, Exact longitudinal equilibrium distribution in the presence of self-fields, *Nuovo Cimento B* **18** (1973) 72.

[10] D. Boussard, Schottky noise and beam transfer function diagnostics, Proc. CERN Accelerator School (CAS) 1985, CERN 87-03 (1987) p. 416.

[11] M. Blaskiewicz *et al.*, Longitudinal impedance of RHIC, Proc. IPAC2015, Richmond, VA, USA, 2015, p. 746.

[12] E. Shaposhnikova *et al.*, Longitudinal peak detected Schottky spectrum, Proc. HB2010, Morschach, Switzerland, 2010, p. 363, TUO1C04.

[13] J. Esteban Muller, Ph.D. thesis, EPFL, Lausanne, Switzerland, 2016.

[14] E. Shaposhnikova *et al.*, Reference measurements of the longitudinal impedance in the CERN SPS, Proc. PAC09, Vancouver, Canada, 2009.

[15] A. Lasheen *et al.*, Single bunch longitudinal instability in the CERN SPS, Proc. IPAC2016, TUPOR009, Busan, Korea, 2016, p.1670.

[16] H. Burkhardt *et al.*, Coherent beam oscillations and transverse impedance in the SPS, Proc. EPAC02, Paris, France, 2002.

[17] E. Shaposhnikova and T. Linnecar, Another method to measure the low-frequency machine impedance, Proc. EPAC96, Sitges, Spain, 1996.

[18] E. Shaposhnikova, Nonlinear bunch motion in an accelerator with reactive impedance, Proc. EPAC96, Sitges, Spain, 1996.

[19] M. A. Allen *et al.*, *IEEE Trans. Nucl. Sci.* **NS-22** (1975) 1838. https://doi.org/10.1109/TNS.1975.4328005

[20] A. Hofmann, Impedance measurements, computations and their interpretation, Proc. EPAC96, Sitges, Spain, 1996, p. 143.

[21] N. S. Sereno *et al.*, A potpourri of impedance measurements at the Advanced Photon Source Storage Ring, Proc. PAC97, 1997, p. 1700.

[22] E. Shaposhnikova *et al.*, Energy loss of a single bunch in the CERN SPS, Proc. EPAC04, Lucerne, Switzerland, 2004, p.1909.

[23] G. Rumolo, Electron cloud, these proceedings.

[24] T. Bohl *et al.*, *Phys. Rev. Lett.* **78** (1997) 3109. https://doi.org/10.1103/PhysRevLett.78.3109

[25] E. Shaposhnikova, Methods of observing the microwave instability above and below transition, Proc. PAC01, Chicago, USA, 2001, p. 385. https://doi.org/10.1109/pac.2001.987521

[26] T. Argyropoulos *et al.*, Identification of the SPS impedance at 1.4 GHz, Proc. IPAC2013, Shanghai, China, 2014, p. 1793.

[27] E. Shaposhnikova *et al.*, Identification of high-frequency resonant impedance in the CERN SPS, Proc. IPAC2014, Dresden, Germany, 2014, p. 1416.

[28] F. Sacherer and F. Pedersen, *IEEE Trans. Nucl. Sci.* **NS-24** (1977) 1393. https://doi.org/10.1109/TNS.1977.4328955

[29] E. Shaposhnikova, Analysis of coupled bunch instability spectra, Proc. Workshop on Instabilities of High Intensity Hadron Beams in Rings, Upton, New York, USA, **496** (1999) 256. https://doi.org/10.1063/1.1301890

[30] A. Chao *et al. Handbook of Accelerator Physics and Engineering*, 2nd ed. (World Scientific, Singapore, 2013). https://doi.org/10.1142/8543